International Journal of Modern Physics A

New Measurements of $B \to PV$ and VV Decays at Belle

Kai-Feng Chen

Physics Department, National Taiwan University,
No.1, Sec. 4, Roosevelt Road, Taipei, Taiwan 106

Received (December 6, 2004)
Revised ()

We present measurements of $B \to PV$ and VV decays based on 140 fb^{-1} of data recorded at the $\Upsilon(4S)$ resonance with the Belle detector at the KEKB e^+e^- storage ring. Branching fractions of $B \to \eta K^*$, $\eta\rho^+$, $\rho\pi^0$, and ρ^+K^* are measured; while upper limits of $B \to \eta\rho^0$ and ρ^0K^* decays are given. The polarization study of $B \to \phi K^*$ is also updated.

1. Introduction

Charmless $B \to PV$ decays provide a large variety sample to study the dynamics of B decays and CP violation. In particular, B decays with η or η' in the final state draw large interest due to the large $B \to \eta' K$ and $B \to \eta K^*$ branching fractions. It was pointed out that two $b \to s$ penguin amplitudes are constructive in $B \to \eta' K$ and $B \to \eta K^*$ but destructive in $B \to \eta' K^*$ and $B \to \eta K$ decays [1]. The $B \to \rho\pi$ decays are occur from $b \to u$ transition and are sensitive to the ϕ_2 angle of the unitarity triangle [2]. Evidence of $B^0 \to \rho^0\pi^0$ channel has been reported by Belle [3] with a rate higher than expectation. Update measurements of those decay modes with more data are required.

The B decays with two vector mesons in the final state provide a rich opportunities to search for CP violation and test of new physics in the correlations between different helicity states. These decays require a sophisticated angular analysis to extract helicity amplitudes. The standard model with factorization assumption predicts the fraction of longitudinal polarization (R_0) should be much bigger than the fraction of transverse polarization (R_T). It is confirmed in the tree dominated $B^+ \to \rho^-\rho^0$ decays. However, the decay $B \to \phi K^*$ which involves the FCNC $b \to s$ transition is in disagreement with the prediction [4]. This provides a strong motivation to update our study with a larger dataset and expend the study to other similar channels, such as $B \to \rho K^*$ decays.

In this report, we use a data sample of 155×10^6 $B\overline{B}$ pairs at the KEKB asymmetric e^+e^- collider with the Belle detector. The Belle detector is a large solid-angle coverage magnetic spectrometer that consists of a silicon vertex detector

(SVD), a central drift chamber (CDC), an array of aerogel Cherenkov counters (ACC), a time-of-flight scintillation counters (TOF), an electromagnetic calorimeter composite of CsI(Tl) crystals (ECL) located inside a superconducting solenoid coil with a 1.5T magnetic field, and a K_L^0 and muon detector (KLM) located outside of the coil.

2. Event Reconstruction and Selection

Reconstructed B meson candidates are chosen by the energy difference $\Delta E = E_B^{\rm cms} - E_{\rm beam}^{\rm cms}$ and the beam energy constrained mass $M_{\rm bc} = \sqrt{(E_{\rm beam}^{\rm cms})^2 - (P_B^{\rm cms})^2}$, where $E_{\rm beam}^{\rm cms}$ is the beam energy in the $\Upsilon(4S)$ center-of-mass (cms) frame, and $E_B^{\rm cms}$ and $P_B^{\rm cms}$ are the cms energy and momentum of the reconstructed B meson, respectively.

The common dominant background to these decay channels comes from $e^+e^- \to q\overline{q}$ ($q = \{u, d, s, c\}$) and tend to be distributed as jet-like. The B signal events are distributed spherically. A set of variables that can characterize the event topology is used to distinguish between signal and continuum background. Those event topology variables such modified Fox-Wolfram moments [?] are combined into a Fisher discriminant $\mathcal{F}$. The angle of the reconstructed B candidate and the beam direction in the cms frame (θ_B) is also included. Those variables, $\mathcal{F}$ and $\cos\theta_B$ are combined into a signal (and background) likelihood variable, which is defined as $\mathcal{L} = \mathcal{L}_{\rm sig(bkg)}(\mathcal{F}) \times \mathcal{L}_{\rm sig(bkg)}(\cos\theta_B)[\times\mathcal{L}_{\rm sig(bkg)}(\cos\theta_H)]$. An additional variable, $\cos\theta_H$, which is defined by the helicity angle of the vector meson in the final state is added for $B \to PV$ decay channels. The continuum background is reduced by a requirement on the likelihood ratio, $\mathcal{R} = \mathcal{L}_{\rm sig}/(\mathcal{L}_{\rm sig} + \mathcal{L}_{\rm bkg})$.

3. Results

3.1. $B \to \eta K^*$ and $B \to \eta\rho$

The signal yields and branching fractions of $B \to \eta K^*$ and $B \to \eta\rho$ decays are obtained by an extended unbinned maximum likelihood (ML) fit on the 2-dimensional space of $M_{\rm bc}$ and ΔE. The likelihood is given by

$$\mathcal{L} = \exp(-\sum_j N_j) \prod_i^N \left[\sum N_j P_j^i(M_{\rm bc}, \Delta E)\right] , \tag{1}$$

where N_j is the yield of category j (signal or continuum background), and P_j^i is probability density for the ith event of that category.

By minimizing the value of $-2\ln(\mathcal{L})$, the branching fractions or upper limits at the 90% confidence level of $B \to \eta K^*$ and $B \to \eta\rho$ decays are obtained to be

$$\begin{aligned}
\mathcal{B}(B \to \eta K^{*0}) &= (19.8^{+2.1}_{-2.0} \pm 1.4) \times 10^{-6} , \\
\mathcal{B}(B \to \eta K^{*+}) &= (22.8^{+3.7}_{-3.5} \pm 2.2) \times 10^{-6} , \\
\mathcal{B}(B \to \eta\rho^{+}) &= (8.5^{+2.6}_{-2.4} \pm 1.0) \times 10^{-6} \ (< 13.0 \times 10^{-6}) ,
\end{aligned}$$

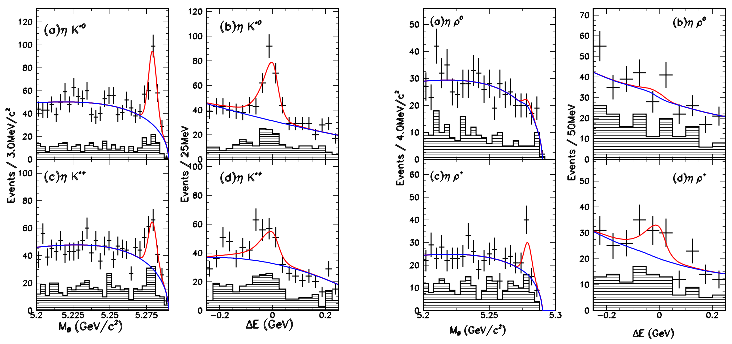

Fig. 1. Projections on $M_{\rm bc}$ and ΔE with the fitting results overlapped for $B \to \eta K^*$ and $B \to \eta\rho$ decays. The shaded area represents $\eta \to \pi^+\pi^-\pi^0$ decays for $B \to \eta K^{*0}$ and $B \to \eta\rho$, and $K^{*+} \to K^0\pi^+$ decays for $B \to \eta K^{*+}$.

$$\mathcal{B}(B \to \eta\rho^0) < 2.7 \times 10^{-6} \ ,$$

where the first error is statistical and the second error is systematic error. The ΔE and $M_{\rm bc}$ projection plots are shown in Figure 1. The direct CP asymmetries are also measured

$$\begin{aligned}
\mathcal{A}_{CP}(B \to \eta K^{*0}) &= -0.04^{+0.11}_{-0.10} \pm 0.01 \ , \\
\mathcal{A}_{CP}(B \to \eta K^{*+}) &= -0.09^{+0.16}_{-0.15} \pm 0.01 \ , \\
\mathcal{A}_{CP}(B \to \eta\rho^{+}) &= -0.17^{+0.33}_{-0.29} \pm 0.02 \ ,
\end{aligned}$$

3.2. $B \to \rho^+\pi^0$ *and* $B \to \rho^0\pi^0$

The same $\Delta E - M_{\rm bc}$ ML fit is used to extract signal yields. The fit includes signal component and background components including continuum events, $b \to c$ decays, $B^0 \to \rho^+\rho^-$ and $B^0 \to \pi^0\pi^0$ decays for $B \to \rho^+\pi^0$ decay. For $B \to \rho^0\pi^0$ mode $b \to c$ decays, $B \to \rho^+\rho^0$, $\rho^+\pi^0$ and $\pi^+\pi^0$ components are included. The probability density functions (PDF) for signal and other charmless B decays are modeled by smoothed 2-dimensional histograms and obtained from large Monte Carlo (MC) samples.

Figure 2 shows the final events sample with a signal yield of 87 ± 15 events for $B \to \rho^+\pi^0$ decay and 15.1 ± 4.8 events for $B \to \rho^0\pi^0$ channel. In order to verify the B signals, the helicity and $M(\pi\pi)$ distributions of the reconstructed ρ-meson candidates are examined. The branching fraction and direct CP asymmetry are measured to be

$$\begin{aligned}
\mathcal{B}(B \to \rho^+\pi^0) &= (13.2 \pm 2.3^{+1.4}_{-1.9}) \times 10^{-6} \ , \\
\mathcal{B}(B \to \rho^0\pi^0) &= (5.1 \pm 1.6 \pm 0.9) \times 10^{-6} \ , \\
\mathcal{A}_{CP}(B \to \rho^+\pi^0) &= 0.06 \pm 0.19^{+0.04}_{-0.06} \ .
\end{aligned}$$

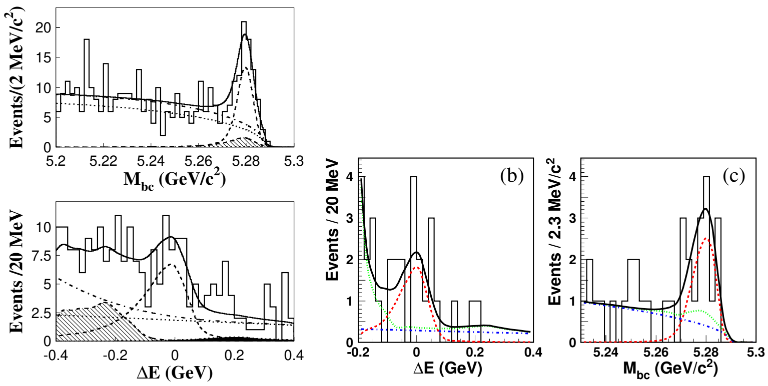

Fig. 2. Projections on $M_{\rm bc}$ and ΔE with the fitting results overlapped for $B \to \rho^+\pi^0$ (left) and $B \to \rho^0\pi^0$ (middle and right) modes.

3.3. $B \to \phi K^*$

The signal fractions are extracted by the same extended unbinned maximum-likelihood fits. The mean and width of the signal PDF are verified using $B \to J/\psi K^*$ decays. Figure 3 shows the ΔE and $M_{\rm bc}$ projections of the B candidates. Furthermore, a full angular analysis is performed with these $B \to \phi K^*$ events. The decay angles of a B-meson to ϕ and K^* vector mesons are defined in the Figure 4. The $\theta_{\rm tr}$ ($\phi_{\rm tr}$) is the polar (azimuthal) angle with respect to the z-axis of the K^+ from ϕ decay in the ϕ rest frame, and θ_{K^*} is defined above.

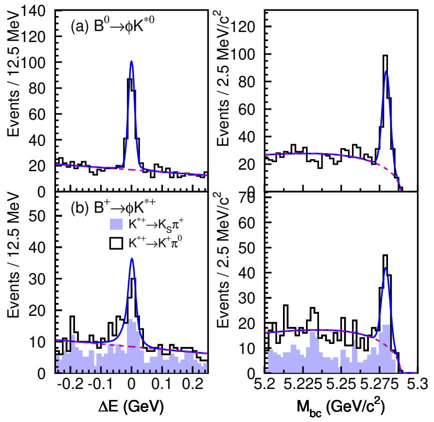

Fig. 3. Distributions of ΔE ($M_{\rm bc}$) with fit results for the events in the M_{bc} (ΔE) signal window.

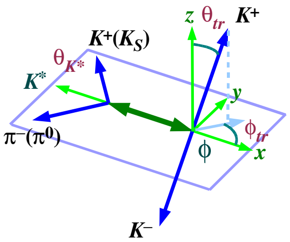

Fig. 4. The definition of decay angles in $B \to \phi K^*$ decays.

The distribution of decays in the three angles is given by

$$\begin{aligned}
\frac{d^3\Gamma(\phi_{\rm tr},\cos\theta_{\rm tr},\cos\theta_{K^*})}{d\phi_{\rm tr}d\cos\theta_{\rm tr}d\cos\theta_{K^*}} &= \frac{9}{32\pi}[|A_\perp|^2 2\cos^2\theta_{\rm tr}\sin^2\theta_{K^*} \\
&+ |A_\parallel|^2 2\sin^2\theta_{\rm tr}\sin^2\phi_{\rm tr}\sin^2\theta_{K^*} \\
&+ |A_0|^2 4\sin^2\theta_{\rm tr}\cos^2\phi_{\rm tr}\cos^2\theta_{K^*} \\
&+ \sqrt{2}{\rm Re}(A_\parallel^* A_0)\sin^2\theta_{\rm tr}\sin 2\phi_{\rm tr}\sin 2\theta_{K^*} \\
&- \eta\sqrt{2}{\rm Im}(A_0^* A_\perp)\sin 2\theta_{\rm tr}\cos\phi_{\rm tr}\sin 2\theta_{K^*} \\
&- 2\eta{\rm Im}(A_\parallel^* A_\perp)\sin 2\theta_{\rm tr}\sin\phi_{\rm tr}\sin^2\theta_{K^*}]\ , \qquad (2)
\end{aligned}$$

where A_0, $A_\parallel$, and $A_\perp$ are the complex amplitudes of the three helicity states in the transversity basis, and $\eta \equiv +1$ (-1) corresponds to B $(\overline{B})$ mesons. A_0 denotes the longitudinal polarization and $A_\perp$ $(A_\parallel)$ is the transverse polarization.

The complex amplitudes are determined by performing an ML fit with the $B \to \phi K^*$ candidates in the signal window. The combined likelihood is given by

$$\begin{aligned}
\mathcal{L} = \prod_i^N \epsilon(\theta_{K^*},\theta_{\rm tr},\phi_{\rm tr})[&f_{\phi K^*}\cdot\Gamma(\theta_{K^*},\theta_{\rm tr},\phi_{\rm tr}) \\
&+ f_{q\overline{q}}\cdot R_{q\overline{q}}(\theta_{K^*},\theta_{\rm tr},\phi_{\rm tr}) \\
&+ f_{KKK^*}\cdot R_{KKK^*}(\theta_{K^*},\theta_{\rm tr},\phi_{\rm tr})]\ , \qquad (3)
\end{aligned}$$

where Γ is the angular distribution function (ADF) given by Eq. 2, and $R_{q\overline{q}}$ and R_{KKK^*} are the ADFs for continuum and $B \to KKK^*$ background, respectively. Figure 5 shows the angle distributions with projections of the fit superimposed. The amplitudes obtained from the fit are shown in Table 1.

Experimentally the following two T-odd [6,7] quantities are used,

$$A_T^0 \equiv \frac{{\rm Im}(A_\perp A_0^*)}{A_0^2 + A_\perp^2 + A_\parallel^2}\ , \qquad A_T^\parallel \equiv \frac{{\rm Im}(A_\perp A_\parallel^*)}{A_0^2 + A_\perp^2 + A_\parallel^2}\ . \qquad (4)$$

The comparison of these triple product asymmetries (A_T^0 and $A_T^\parallel$) with the corresponding quantities for the CP-conjugated decays ($\overline{A}_T^0$ and $\overline{A}_T^\parallel$) provide a true T-violating measurement. Several additional variables that can be measured through

Table 1. The amplitudes obtained from the angular analysis, where the first errors are statistical and the second errors are systematic.

Mode	ϕK^{*0}	ϕK^{*+}	Combined
$\lvert A_0\rvert^2$	$0.52 \pm 0.07 \pm 0.05$	$0.49 \pm 0.13 \pm 0.05$	$0.51 \pm 0.06 \pm 0.04$
$\lvert A_\perp\rvert^2$	$0.30 \pm 0.07 \pm 0.03$	$0.12^{+0.11}_{-0.08} \pm 0.03$	$0.24 \pm 0.06 \pm 0.03$
$arg(A_\parallel)$ (rad)	$-2.30 \pm 0.28 \pm 0.04$	$-2.07 \pm 0.34 \pm 0.07$	$-2.21 \pm 0.22 \pm 0.05$
$arg(A_\perp)$ (rad)	$0.64 \pm 0.26 \pm 0.05$	$0.93^{+0.55}_{-0.39} \pm 0.12$	$0.72 \pm 0.21 \pm 0.06$

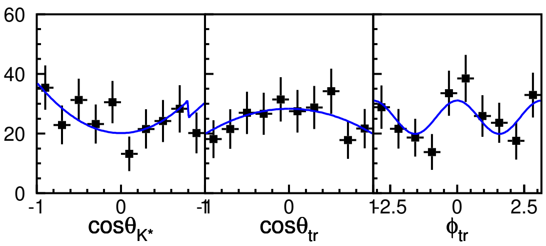

Fig. 5. Projections of the transversity angles with results of the fit superimposed. The points with error bars show the efficiency corrected data after subtraction of continuum and $B \to K^+K^-K^*$ background. The discontinuity in the fit to $\cos\theta_{K^*}$ is due to the requirement of $\cos\theta_{K^*} < 0.8$ in $B^+ \to \phi K^{*+}(K^{*+} \to K^+\pi^0)$ decay.

angular analysis are suggested in Ref. [8]. The following equation should be held in the absence of NP:

$$\Sigma_{\lambda\lambda} = \Sigma_{\parallel 0} = \Lambda_{\perp i} = 0 \ . \tag{5}$$

Any violation of this relation would be an evidence of NP.

By separating B-meson and $\overline{B}$-meson samples in the unbinned maximum likelihood fit, we obtain the helicity amplitudes for the B and $\overline{B}$ samples, the triple-product correlations, and other NP-sensitive observables, are given in Table 2 and 3.

Table 2. The measured helicity amplitudes and triple-product correlations in the B-meson and $\overline{B}$-meson samples.

Mode	B-meson combined (ϕK^{*0} and ϕK^{*+})	$\overline{B}$-meson combined ($\phi\overline{K}^{*0}$ and ϕK^{*-})
$\lvert A_0\rvert^2$	$0.41 \pm 0.10 \pm 0.03$	$0.59 \pm 0.08 \pm 0.06$
$\lvert A_\perp\rvert^2$	$0.24 \pm 0.10 \pm 0.02$	$0.26 \pm 0.08 \pm 0.04$
$arg(A_\parallel)$ (rad)	$-2.29 \pm 0.35 \pm 0.13$	$-2.05 \pm 0.31 \pm 0.04$
$arg(A_\perp)$ (rad)	$0.74 \pm 0.31 \pm 0.10$	$0.81 \pm 0.31 \pm 0.06$
A_T^0	$0.21 \pm 0.08 \pm 0.03$	$0.28 \pm 0.09 \pm 0.05$
$A_T^\parallel$	$0.04 \pm 0.08 \pm 0.02$	$0.06 \pm 0.06 \pm 0.02$

Table 3. The observables sensitive to NP extracted from angular analysis.

Λ Observables			Σ Observables		
Λ_{00}	$=$	$0.50 \pm 0.06 \pm 0.04$	Σ_{00}	$=$	$-0.09 \pm 0.06 \pm 0.02$
$\Lambda_{\parallel\parallel}$	$=$	$0.25 \pm 0.06 \pm 0.02$	$\Sigma_{\parallel\parallel}$	$=$	$0.10 \pm 0.06 \pm 0.02$
$\Lambda_{\perp\perp}$	$=$	$0.25 \pm 0.06 \pm 0.03$	$\Sigma_{\perp\perp}$	$=$	$-0.01 \pm 0.06 \pm 0.02$
$\Lambda_{\perp 0}$ $(= \mathcal{A}_T^0)$	$=$	$0.07 \pm 0.11 \pm 0.04$	$\Sigma_{\perp 0}$	$=$	$-0.49 \pm 0.12 \pm 0.07$
$\Lambda_{\perp\parallel}$ $(= \mathcal{A}_T^{\parallel})$	$=$	$0.02 \pm 0.10 \pm 0.03$	$\Sigma_{\perp\parallel}$	$=$	$-0.09 \pm 0.10 \pm 0.02$
$\Lambda_{\parallel 0}$	$=$	$-0.39 \pm 0.13 \pm 0.06$	$\Sigma_{\parallel 0}$	$=$	$-0.11 \pm 0.13 \pm 0.04$

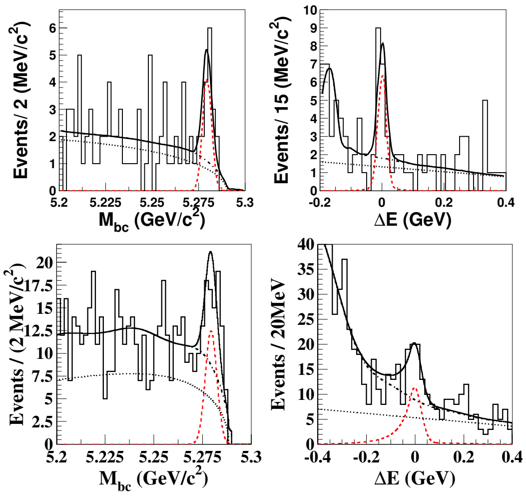

Fig. 6. Projections on $M_{\rm bc}$ and ΔE with the fit results overlapped for $B^0 \to \rho^0 K^{*0}$ (top) and $B^+ \to \rho^+ K^{*0}$ (bottom) decays.

3.4. $B \to \rho K^{*0}$

The signal yields are extracted by applying a ML fit to ΔE and $M_{\rm bc}$ distributions. The fit includes components for signal, continuum background, and $b \to c$ decays. We find 14.1 ± 4.4 $B \to K^+\pi^-\pi^+\pi^-$ events and 56.5 ± 11.6 $B \to K^+\pi^-\pi^+\pi^0$ events. The ΔE and $M_{\rm bc}$ distributions and fit results are shown in Figure 6. However, this fit cannot distinguish the $B \to \rho K^{*0}$ signal from non-resonant decays, such as $B \to \rho K^+\pi^0$ or $B \to \pi\pi K^{*0}$ modes. Therefore, the $B \to \rho K^{*0}$ signal yields are extracted by fitting to the $M(K\pi)$ and $M(\pi\pi)$ invariant masses for the events located inside of ΔE and $M_{\rm bc}$ signal region.

For the signal $B^0 \to \rho^0 K^{*0}$, a two-dimensional ML fit to $M(K\pi)$ and $M(\pi\pi)$ is performed and found 0.0 ± 5.2 events, and yield of $B^0 \to f_0(980)K^{*0}$ is found to be $10.2^{+5.3}_{-4.4}$ events. Hence we provide an upper limit of this decay

$$\mathcal{B}(B^0 \to \rho^0 K^{*0}) < 2.6^{-6} \ , \tag{6}$$

$$\mathcal{B}(B^0 \to f_0(980) K^{*0}) < 5.2^{-6} \ , \tag{7}$$

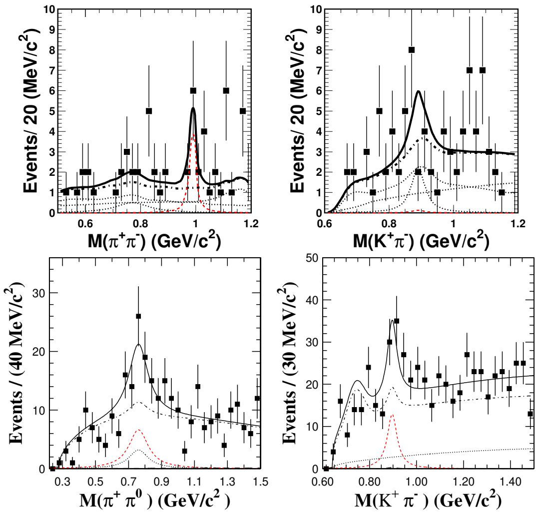

Fig. 7. Projections on $M(K\pi)$ and $M(\pi\pi)$ with the fit results overlapped for $B^0 \to \rho^0 K^{*0}$ (top) and $B^+ \to \rho^+ K^{*0}$ (bottom) decays.

at 90% confidence level. Figure 7 shows the invariant mass distributions of $B^0 \to \rho^0 K^{*0}$ candidates with fit results overlapped.

The signal yield of the other decay channel $B^+ \to \rho^+ K^{*0}$ is also extracted by a 2D ML fit to the $M(K\pi)$ and $M(\pi\pi)$ distributions and found to be 26.6 ± 8.7 events. The results are also shown in Figure 7. Therefore we perform an angular analysis to the helicity angle distributions of $\rho^+ \to \pi^+\pi^0$ and $K^{*0} \to K^+\pi^-$ decays to determine the helicity components. For the longitudinal polarization case, the distribution is proportional to $\cos^2\theta_\rho \times \cos^2\theta_{K^*}$, and is proportional to $\sin^2\theta_\rho \times \sin^2\theta_{K^*}$ for the transverse polarization. An unbinned 2D ML fit to the helicity angle distributions is used to extract the helicity components. The fraction of longitudinal polarization is determined to be

$$R_0(B^+ \to \rho^+ K^{*0}) = 0.50 \pm 0.19^{+0.05}_{-0.07} \ . \tag{8}$$

Projections of the helicity angles are shown in the Figure 8. Based on this measurement, the reconstruction efficiency is determined and the branching fraction is measured to be

$$\mathcal{B}(B^0 + \to \rho^+ K^{*0}) = (6.6 \pm 2.2 \pm 0.8)^{-6} \ . \tag{9}$$

Acknowledgments

We thank the KEKB group for the excellent operation of the accelerator, the KEK Cryogenics group for the efficient operation of the solenoid, and the KEK computer group and the NII for valuable computing and Super-SINET network support.

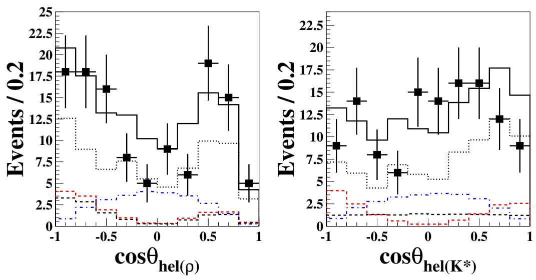

Fig. 8. The helicity angle distributions of $\rho^+ \to \pi^+\pi^0$ and $K^{*0} \to K^+\pi^-$ decays with the results of fit overlapped.

We acknowledge support from MEXT and JSPS (Japan); ARC and DEST (Australia); NSFC (contract No. 10175071, China); DST (India); the BK21 program of MOEHRD and the CHEP SRC program of KOSEF (Korea); KBN (contract No. 2P03B 01324, Poland); MIST (Russia); MESS (Slovenia); Swiss NSF; NSC and MOE (Taiwan); and DOE (USA).

References

1. M.-Z. Yang and Y.D. Yang, Nucl. Phys. B **609**, 469 (2001); M. Beneke and M. Neubert, Nucl. Phys. B **651**, 225 (2002); D. Du, *et. al.* Phys. Rev. D **65** 094025 (2002).
2. N. Cabibbo, Phys. Rev. Lett. **10**, 531 (1963); M. Kobayashi and T. Maskawa, Prog. Theor. Phys. **49**, 652 (1973).
3. K. Abe, *et. al.* (Belle Collaboration), Phys. Rev. D **66** 071102 (2002).
4. K.-F.Chen, *et. al.* (Belle Collaboration),Phys. Rev. Lett. **91**, 201801 (2003).
5. The Fox-Wolfram moments were introduced in G.C. Fox, S. Wolfram, Phys. Rev. Lett. **41** (1978) 1581 ; The use of the modified Fox-Wolfram moments was first proposed in a series of lectures on continuum suppression at KEK by R. Enomoto in May and June, 1999.
6. A. Datta and D. London, hep-ph/0303159.
7. We take the definitions of $A_T^0 = A_T^{(1)}$ and $A_T^{\parallel} = A_T^{(2)}$, but $\overline{A}_T^0 = -\overline{A}_T^{(1)}$ and $\overline{A}_T^{\parallel} = -\overline{A}_T^{(2)}$. The variables $A_T^{(1)}$ and $A_T^{(2)}$ are defined in Ref. [6].
8. D. London, N. Sinha and R. Sinha. hep-ph/0402214.